

# Reconfigurable Intelligent Surface-Aided Spectrum Sharing Coexisting with Multiple Primary Networks

Zhong Tian, Zhengchuan Chen, Min Wang, Yunjian Jia, and Shi Jin

## Abstract

In the spectrum sharing system (SSS) coexisting with multiple primary networks, a well-designed reconfigurable intelligent surface (RIS) is employed to control the radio environments of wireless channels and relieve the scarcity of the spectrum resource in this work, which can realize high spectral efficiency (SE) and energy efficiency (EE). Specifically, the SE enhancement in the considered SSS is decomposed into two subproblems which are a second-order programming (SOP) and a fractional programming of the convex quadratic form (CQFP), respectively, to optimize alternatively the beam-forming vector at the secondary access point and the reflecting coefficients at the RIS. The CQFP subproblem about optimizing the reflecting coefficients can be solved by the domain and envelope shrinking algorithm (DES), providing the best SE performance. Besides, a low-complexity method of gradient-based linearization with domain (GLD) is proposed for obtaining a sub-optimal reflecting coefficients for fast deployment. Considering the power consumption in the practical application of RIS-aided SSS, the EE performance of our proposed GLD method has significant gain over that of the SSS without RIS. The simulation results indicate the effectiveness of the DES algorithm and show that the GLD method improves the SE and EE performance in RIS-aided SSS with multiple primary networks.

## Index Terms

Reconfigurable intelligent surface, spectral efficiency, energy efficiency.

Z. Tian, Z. Chen, and Y. Jia are with the School of Microelectronics and Communication Engineering, Chongqing University, Chongqing, China (e-mail: ztian@cqu.edu.cn).

M. Wang is with School of Optoelectronics Engineering, Chongqing University of Posts and Telecommunications, Chongqing, China.

S. Jin is with the National Mobile Communications Research Laboratory, Southeast University, Nanjing, China.

## I. INTRODUCTION

In the 6G era [1], it is predicted that the amount of global mobile traffic increases from 66 Exabytes per month in 2020 to 5016 Exabytes per month in 2030 [2]. Virtual reality (VR) devices may need the transmit rate by 10 Gbps to satisfy the high quality of experience (QoE) for the customers. The rapid development of digital economy and the emerging applications in consumption and business stimulate the tremendous demands about the enhancement of data transmission. Spectrum resource is a non-negligible bottleneck to improve the efficiency of data transmission between the transceivers, which is the original motivation of spectrum sharing technology (also called cognitive radios) [3]. In the scenarios of spectrum sharing, the secondary access points (S-APs) always seek for the opportunities to transmit the data to the secondary users (SUs) without decreasing the quality of service (QoS) between primary access points (P-APs) and the primary users (PUs) in the primary networks. Several primary networks coexist in the same spectrum band of citizen broadband radio service (CBRS) [4], inducing the data transmissions of secondary networks more complicated. To support the high rate of data transmission and alleviate the power consumption in communications, both spectral efficiency (SE) and energy efficiency (EE) of the secondary network should be optimized.

Recently, reconfigurable intelligent surface (RIS) [5][6] shows the capability to control and optimize the radio environments of wireless channels between transceivers, which could be utilized to improve the SE [7] and EE [8] [9]. The wireless communication prototype based on RIS was developed in [10], which has a new type of high-gain yet low-cost RIS with 256 elements. For the downlink transmission to cell-edge users at the cell boundary of multiple cells aided by the RIS, the weighted sum rate of all users was maximized by jointly optimizing the active precoding matrices at the APs and the phase shifts at the RISs in [11] with the methods of block coordinate descent (BCD), majorization-minimization (MM) and the complex circle manifold. Besides, the wideband RIS-aided cell-free network was investigated in [12] to maximize the network capacity with joint precoding design at APs and RISs. Moreover, the downlink multigroup multicast communication systems were assisted by the RIS to obtain better performance on SE and EE in [13].

RIS can also be combined with some existing technologies to obtain the enhancement on the performance. To support the sustainable working mode, an analytical framework for the statistical analysis of the battery recharging time (BRT) in RIS-aided wireless power transfer

(WPT) systems was proposed in [14]. The problem about passive beamforming and information transfer for multiuser multiple-input multiple-output (MU-MIMO) systems aided by the RISs was investigated in [15] by utilizing the iterative algorithm based on sample average approximation for efficient passive beamforming design and the turbo message passing algorithm for the bilinear estimation problem at the receiver. The unified communication-learning optimization problem about device selection, over-the-air transceiver design and RIS configuration in federated learning is solved by the learning analysis framework proposed in [16] where RIS is leveraged to strengthen the weak channels for the bottleneck of the model aggregation performance. Besides, an iterative resource allocation algorithm was proposed in RIS-aided federated learning system to realize high EE [17]. The intelligent spectrum learning with the trained convolutional neural network was investigated in [18] to reduce the interfering signals in the received signals reflected from the RIS and maximize the signal-to interference-plus-noise (SINR) by dynamically activating the binary status of the RIS elements. The deep reinforcement learning-based algorithm was developed to jointly design the transmit beamforming matrix at the base station and the phase shift matrix at the RIS simultaneously in massive MIMO systems [19].

As far as we know, the first demo system of RIS-assisted spectrum sharing system (SSS) was presented in [20] to increase the indoor network capacity significantly and relieve the overly crowded situation of spectrum resource, where multiple users can share the same spectrum band without interfering each other by controlling the reflecting coefficients at the RIS. For multiple scenarios about the deployments of the RIS embedded in the basic SSS, the optimization for reflecting coefficients at the RIS and the power allocation of the S-AP are jointly designed with successive convex approximation (SCA) [21]. MIMO [22][23] and full duplex [24] are also introduced as extra resources to improve SE of the SSSs assisted by RIS more aggressively.

When multiple primary networks are involved in the SSS, the RIS and APs configured with multiple antennas provide more capability for the enhancement of SE performance, which also introduce more complicated coupling of optimizing variables between primary networks and secondary networks in the optimization of the system performance. Hence, the effective methods should be carefully investigated to control the parameters and variables at the S-AP and the RIS. Besides, the problem of power consumption or EE should also be considered for the RIS-aided spectrum sharing system. In particular, the discretization of the reflecting coefficients at the RIS is another concern for the practical consideration about the hardware of the RIS device.

In this paper, we focus on the enhancement of SE and EE for the SSS with multiple primary

networks by utilizing the RIS to manipulate the radio environment of the wireless channels, which can relieve the interference between primary networks and secondary networks with well-designed parameters. To maximize the achievable rate of the SU, we optimize the reflecting coefficients at the RIS and the beamforming vector at the S-AP under the power constraints of the interferences from the S-AP to the PUs. With the reflecting coefficients at the RIS fixed, we transform the optimization about the beamforming vector at the S-AP for the achievable rate of the SU equivalently as a second-order programming (SOP). While the beamforming vector of the S-AP is fixed in the SSS, we model the optimization of the achievable rate of the SU as the fractional programming with convex quadratic form (CQFP) and design useful algorithms to find the optimal reflecting coefficients. With RIS involved in the SSS, the EE performance of the secondary network is also investigated to reveal the advantages of the passive beamforming from RIS.

The main contributions of this paper can be summarized as follows:

- A new system model about RIS-assisted SSS coexisting with multiple primary networks is established, based on which the problem about optimizing the achievable rate of the SU is split into two subproblems including the SOP and the CQFP. In particular, the coupling between the RIS and the interferences in the SSS is presented clearly in the process of the problem formulation.
- For maximizing the achievable rate of the SU in the SSS, alternative optimization (AO) is utilized to solve the subproblems (the SOP and the CQFP). For optimizing the beamforming vector at the S-AP of the SOP, the subproblem is transformed equivalently into a concave problem and solved by standard convex optimization tools (such as interior point method). For the CQFP, we propose the domain and envelope shrinking (DES) algorithm to obtain the optimal solution of the reflecting coefficients at the RIS. Specifically, in each iteration of the proposed DES algorithm, it computes and outputs convergent upper and lower bounds for the objective value of CQFP, providing trackable and effective solution close to the optimal solution.
- To decrease the computation complexity, the method of gradient-based linearization with domain (GLD) is proposed to obtain a sub-optimal solution for the CQFP subproblem on optimizing reflecting coefficients. The achievable rate of GLD method can have good approximation to the optimal objective value of the proposed DES, which also shows obvious gain over the achievable rate of the compared semidefinite programming (SDP) method.

- The EE performance of the RIS-aided secondary network is considered for practical applications, which shows that RIS-aided SSS can obtain significant gain on EE and reduce the transmit power consumption of the S-AP by passive beamforming. The method of nearest point searching with penalty (NPSP) is also proposed to realize the discrete quantization on the phase shifts of the RIS for the practical consideration. It is demonstrated that the NPSP can have little loss on the performance of achievable rate of the SU compared with those used in the case with the continuous value of the phase shifts of the RIS.

The remaining sections of this paper are organized as follows. The system model and the problem of RIS-assisted spectrum sharing coexisting with multiple primary networks are formulated in Section II. The AO on the beamforming vector at the S-AP and the reflecting coefficients at the RIS is illustrated in Section III. The practical considerations about EE performance and the discretization of reflecting coefficients on the RIS are investigated in Section IV. The simulation results and discussions about SE and EE performance of RIS-assisted SSS with multiple primary networks are presented in Section V. The conclusions of this paper are drawn in Section VI.

**Notations:** The scalars, column vectors, and matrices are shown as a lower case  $b$ , boldface lower case  $\mathbf{b}$ , and boldface upper case letter  $\mathbf{B}$ , respectively. For vector  $\boldsymbol{\theta}$ ,  $\text{diag}(\boldsymbol{\theta})$  gives a diagonal matrix whose  $n$ -th diagonal element is  $[\boldsymbol{\theta}]_n$  (the  $n$ -th element of  $\boldsymbol{\theta}$ ). For matrix  $\mathbf{B}$ ,  $\mathbf{B}^T$  and  $\mathbf{B}^H$  denote its transpose and complex conjugate transpose.  $\mathbf{B} \succeq 0$  or  $\mathbf{B} \succ 0$  means that  $\mathbf{B}$  is a positive semidefinite (PSD) matrix or a positive definite (PD) matrix.  $\mathbf{A} \otimes \mathbf{B}$  denotes the Kronecker product between  $\mathbf{A}$  and  $\mathbf{B}$ .  $\mathcal{CN}(0, \sigma^2)$  denotes the distribution of a circularly symmetric complex Gaussian random variable.  $\mathbf{I}_M$  denotes the  $M$ -dimensional identity matrix.  $\angle(\cdot)$  denotes the angle of a complex number.

## II. SYSTEM MODEL

In this paper, the RIS-assisted SSS with multiple primary networks is considered. The SU in the secondary network and the PUs in multiple primary networks are assumed to be distributed randomly near the RIS. For example, the SSS with two primary networks is shown in Fig. 1. Besides of the direct links ( $D_{p1}$ ,  $D_{p2}$ ,  $D_{p1,b}$ , and  $D_{p2,b}$ ) from the P-APs to the PUs or the SU, the transmit signals of the P-APs can also be reflected by the RIS, with the cascaded links to the PUs or the SU ( $F_{p1}$ ,  $F_{p2}$ ,  $F_{p1,b}$  and  $F_{p2,b}$ ) in Fig. 1. For the S-AP, the transmit signals to the SU or the PUs also include the direct links to the SU or the PUs ( $D_s$ ,  $D_{s,1}$  and  $D_{s,2}$ ) and the cascaded links reflected by the RIS ( $F_s$ ,  $F_{s,1}$  and  $F_{s,2}$ ) in Fig. 1.

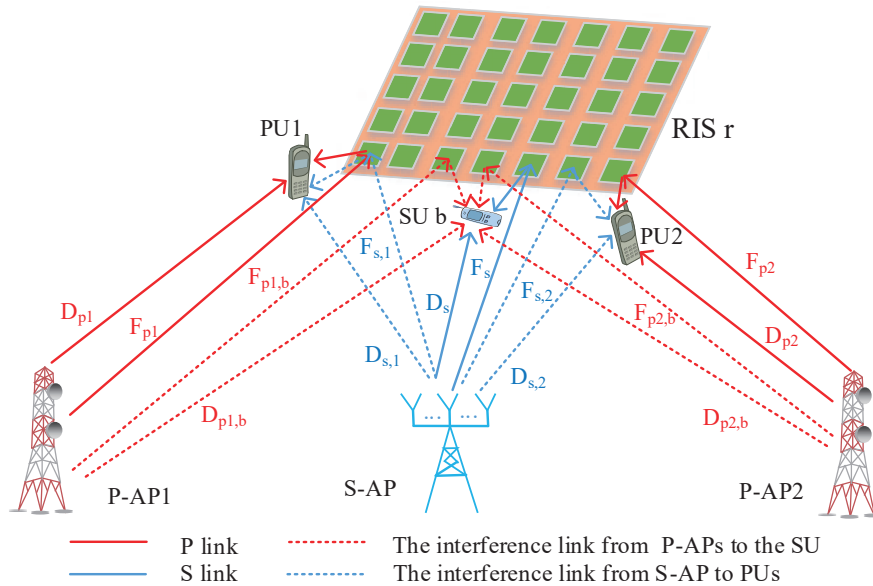


Fig. 1. The RIS-assisted spectrum sharing system coexisting with two primary networks.

Assume that  $J$  primary networks and one secondary network coexist in the SSS. Each primary network includes one P-AP and one PU, configured with a single antenna respectively. Moreover, the secondary network includes one S-AP with  $M$  antennas and one SU with a single antenna. Assuming  $\boldsymbol{\theta} = [\bar{\beta}_1 e^{i\bar{\phi}_1}, \dots, \bar{\beta}_N e^{i\bar{\phi}_N}]^T$  composed with the reflecting amplitude  $\bar{\beta}_n$  and the phase shift  $\bar{\phi}_n$  of  $n$ -th element on RIS ( $n \in \mathcal{N} = \{1, \dots, N\}$ ), the reflecting coefficients of IRS are expressed as diagonal matrix  $\boldsymbol{\Theta} = \text{diag}(\boldsymbol{\theta})$ .

#### A. The Channel Models about the Direct Link and the Cascaded Link Reflected by RIS

The RIS-assisted SSS with multiple primary networks makes the channels between the sources (the P-APs and S-AP) and the destinations (the PUs and the SU) more complicated. The direct link from the source to the destination usually can be modeled as Rayleigh channel. Let  $h_j$  and  $h_{p_j,b}$  ( $j \in \mathcal{J} = \{1, \dots, J\}$ ) denote the channels of the direct links from  $j$ -th P-AP to the  $j$ -th PU and the SU, respectively, which are independent and identically distributed (i.i.d) complex Gaussian random variable with the zero mean and different variances, namely,  $h_j \sim \mathcal{CN}(0, \sigma_j^2)$  and  $h_{p_j,b} \sim \mathcal{CN}(0, \sigma_{p_j,b}^2)$ . For the direct links from the S-AP to the PUs and the SU, the channels are denoted as  $\mathbf{h}_{s,j} \sim \mathcal{CN}(0, \sigma_{s,j}^2 \mathbf{I}_M)$  and  $\mathbf{h}_s \sim \mathcal{CN}(0, \sigma_s^2 \mathbf{I}_M)$ , respectively.

The channels reflected by the RIS from the source to the destination can be modeled as cascaded channels. The cascaded channel from the  $j$ -th P-AP to the  $j$ -th PU is denoted as  $\mathbf{h}_{r,j}^H \boldsymbol{\Theta} \mathbf{h}_{p_j,r}$  where  $\mathbf{h}_{p_j,r} \in \mathbb{C}^{N \times 1}$  and  $\mathbf{h}_{r,j} \in \mathbb{C}^{N \times 1}$  are the channels from  $j$ -th P-AP to the RIS and

from the RIS to the  $j$ -th PU, respectively. Similarly,  $\mathbf{h}_{r,j}^H \Theta \mathbf{H}_{s,r}$ ,  $\mathbf{h}_{r,b}^H \Theta \mathbf{H}_{s,r}$ , and  $\mathbf{h}_{r,b}^H \Theta \mathbf{h}_{p_j,r}$  denote the cascaded channels reflected by RIS from the S-AP to  $j$ -th PU, from the S-AP to the SU, and from the  $j$ -th P-AP to the SU, respectively.  $\mathbf{H}_{s,r} \in \mathbb{C}^{N \times M}$  and  $\mathbf{h}_{r,b} \in \mathbb{C}^{N \times 1}$  refer to the channels from the S-AP to the RIS and from the RIS to the SU, respectively.

The RIS is usually deployed near the APs or the users to have obvious impact on the performance of the system [25]. The channels between RIS and the APs or the users can be modeled as Rician fading. For example, the channel  $\mathbf{h}_{p_j,r}$  can be modeled as

$$\mathbf{h}_{p_j,r} = \sqrt{\frac{\kappa_1}{1 + \kappa_1}} \mathbf{f}_{p_j,r}^{\text{LOS}} + \sqrt{\frac{1}{1 + \kappa_1}} \mathbf{f}_{p_j,r}^{\text{NLOS}}, \quad 0 \leq \kappa_1, \quad (1)$$

where  $\mathbf{f}_{p_j,r}^{\text{LOS}} \in \mathbb{C}^{N \times 1}$  and  $\mathbf{f}_{p_j,r}^{\text{NLOS}} \in \mathbb{C}^{N \times 1}$  are the components of line-of-sight and non-line-of-sight paths, respectively. The elements of  $\mathbf{f}_{p_j,r}^{\text{NLOS}}$  are i.i.d. complex Gaussian distribution with zero means and the same variances. Similarly, the channels  $\mathbf{H}_{s,r}$ ,  $\mathbf{h}_{s,j}$  and  $\mathbf{h}_{s,b}$  can be shown as

$$\mathbf{H}_{s,r} = \sqrt{\frac{\kappa_2}{1 + \kappa_2}} \mathbf{F}_{s,r}^{\text{LOS}} + \sqrt{\frac{1}{1 + \kappa_2}} \mathbf{F}_{s,r}^{\text{NLOS}}, \quad 0 \leq \kappa_2, \quad (2)$$

$$\mathbf{h}_{r,j} = \sqrt{\frac{\kappa_3}{1 + \kappa_3}} \mathbf{f}_{r,j}^{\text{LOS}} + \sqrt{\frac{1}{1 + \kappa_3}} \mathbf{f}_{r,j}^{\text{NLOS}}, \quad 0 \leq \kappa_3, \quad (3)$$

$$\mathbf{h}_{r,b} = \sqrt{\frac{\kappa_4}{1 + \kappa_4}} \mathbf{f}_{r,b}^{\text{LOS}} + \sqrt{\frac{1}{1 + \kappa_4}} \mathbf{f}_{r,b}^{\text{NLOS}}, \quad 0 \leq \kappa_4. \quad (4)$$

According to [26], we have

$$\mathbf{f}_{p_j,r}^{\text{LOS}} = \mathbf{a}_r(\alpha_{\text{AoA},p_j}, \beta_{\text{AoA},p_j}), \quad (5)$$

$$\mathbf{f}_{r,j}^{\text{LOS}} = \mathbf{a}_r(\alpha_{\text{AoD},j}, \beta_{\text{AoD},j}), \quad (6)$$

$$\mathbf{F}_{s,r}^{\text{LOS}} = \mathbf{a}_r(\alpha_{\text{AoA},s}, \beta_{\text{AoA},s})(\mathbf{a}_s(\alpha_{\text{AoD},s}))^H, \quad (7)$$

$$\mathbf{f}_{r,b}^{\text{LOS}} = \mathbf{a}_r(\alpha_{\text{AoD},b}, \beta_{\text{AoD},b}). \quad (8)$$

$\mathbf{a}_r(\alpha_{\text{AoA}}, \beta_{\text{AoA}}) = \mathbf{a}_r^{(N_1)}(\alpha_{\text{AoA}}, \beta_{\text{AoA}}) \otimes \mathbf{a}_r^{(N_2)}(\alpha_{\text{AoA}}, \beta_{\text{AoA}})$  represents the steering vector for RIS in (5)–(8), where  $N_1$  and  $N_2$  are the number of elements in a single row and a single column at the RIS, respectively.  $\alpha_{\text{AoA}}$  and  $\beta_{\text{AoA}}$  denote the azimuthal angle of arrival (AoA) and elevation AoA, respectively. Similarly,  $\alpha_{\text{AoD}}$  and  $\beta_{\text{AoD}}$  denote the azimuthal angle of departure (AoD) and elevation AoD, respectively. Furthermore, the elements of  $\mathbf{a}_r^{(N_1)}(\cdot, \cdot)$ ,  $\mathbf{a}_r^{(N_2)}(\cdot, \cdot)$  and  $\mathbf{a}_s(\cdot)$  are calculated as

$$[\mathbf{a}_r^{(N_1)}(\alpha, \beta)]_{n_1} = e^{i \frac{2(n_1-1)\pi d}{\lambda} \cos(\beta) \cos(\alpha)}, \quad n_1 \in \mathcal{N}_1,$$

$$[\mathbf{a}_r^{(N_2)}(\alpha, \beta)]_{n_2} = e^{-i \frac{2(n_2-1)\pi d}{\lambda} \cos(\beta) \sin(\alpha)}, \quad n_2 \in \mathcal{N}_2,$$

$$[\mathbf{a}_s(\alpha)]_m = e^{i\frac{2(m-1)\pi d}{\lambda}\sin(\alpha)}, m \in \mathcal{M} = \{1, \dots, M\},$$

where  $\mathcal{N}_1 = \{1, \dots, N_1\}$  and  $\mathcal{N}_2 = \{1, \dots, N_2\}$ .

In this paper, the perfect channel state information (CSI) is assumed to be known. We focus on the methods for improving the SE performance of the SU in the RIS-assisted SSS coexisting with multiple primary networks.

### B. The Maximization on the Achievable Rate of the SU

The receiving signal of the PU in  $j$ -th primary network is expressed by

$$\begin{aligned} y_j &= (\mathbf{h}_{r,j}^H \Theta \mathbf{h}_{p_j,r} + h_j) \sqrt{P_j} x_j \\ &+ (\mathbf{h}_{r,j}^H \Theta \mathbf{H}_{s,r} + \mathbf{h}_{s,j}^H) \mathbf{v}_s x_s + z_j, j \in \mathcal{J}, \end{aligned} \quad (9)$$

where  $P_j$ ,  $x_j$ ,  $\mathbf{v}_s$  and  $z_j$  denote the transmit power of the  $j$ -th P-AP, the transmit symbol of the  $j$ -th P-AP, the beamforming vector of the S-AP and the white Gaussian noise at the  $j$ -th PU with  $z_j \sim \mathcal{CN}(0, \sigma_{z_j}^2)$ , respectively. The receiving signal of the SU is shown as

$$\begin{aligned} y_b &= (\mathbf{h}_{r,b}^H \Theta \mathbf{H}_{s,r} + \mathbf{h}_s^H) \mathbf{v}_s x_s \\ &+ \sum_{j=1}^J (\mathbf{h}_{r,b}^H \Theta \mathbf{h}_{p_j,r} + h_{p_j,b}) \sqrt{P_j} x_j + z_b, \end{aligned} \quad (10)$$

where  $x_s$  and  $z_b$  denote the transmit symbol of the S-AP and the white Gaussian noise at the SU with  $z_b \sim \mathcal{CN}(0, \sigma_{z_b}^2)$ , respectively. Then, the SINR of the SU is denoted by

$$\gamma_b = \frac{|(\mathbf{h}_{r,b}^H \Theta \mathbf{H}_{s,r} + \mathbf{h}_s^H) \mathbf{v}_s|^2}{\sum_{j=1}^J P_j |\mathbf{h}_{r,b}^H \Theta \mathbf{h}_{p_j,r} + h_{p_j,b}|^2 + \sigma_b^2}, \quad (11)$$

where  $\sum_{j=1}^J P_j |\mathbf{h}_{r,b}^H \Theta \mathbf{h}_{p_j,r} + h_{p_j,b}|^2$  is the superposed interference from P-APs. Since the secondary network is an interference-limited system, the noise part in  $\gamma_b$  can be ignored. Therefore, SINR in (11) can be simplified as SIR. The interference from the S-AP to the  $j$ -th PU can be denoted by

$$\Gamma_j = |(\mathbf{h}_{r,j}^H \Theta \mathbf{H}_{s,r} + \mathbf{h}_{s,j}^H) \mathbf{v}_s|^2, j \in \mathcal{J}, \quad (12)$$

where  $\Gamma_j$  is limited to guarantee that the interference from S-AP has little impact on the communications in  $j$ -th primary network. Then, the maximization of the achievable rate of the SU can be formulated as

$$\text{P0: } \max_{\hat{\boldsymbol{\theta}}, \mathbf{v}_s} \log_2 \left( 1 + \frac{\hat{\boldsymbol{\theta}}^H (\hat{\mathbf{H}}_s \mathbf{v}_s \mathbf{v}_s^H \hat{\mathbf{H}}_s^H) \hat{\boldsymbol{\theta}}}{\hat{\boldsymbol{\theta}}^H (\sum_{j=1}^J P_j \tilde{\Phi}_{j,b}) \hat{\boldsymbol{\theta}}} \right) \quad (13a)$$

$$\text{s.t. } |\hat{\boldsymbol{\theta}}^H \hat{\mathbf{H}}_{s,j} \mathbf{v}_s|^2 \leq \bar{\Gamma}_j, j \in \mathcal{J}, \quad (13b)$$

$$|[\hat{\boldsymbol{\theta}}]_n| \leq 1, n \in \mathcal{N}, \quad (13c)$$

$$[\hat{\boldsymbol{\theta}}]_{N+1} = 1, \quad (13d)$$

$$\|\mathbf{v}_s\|^2 \leq P_{\max}, \quad (13e)$$

where  $\hat{\boldsymbol{\theta}}^H = [\boldsymbol{\theta}^H \ 1]$ ,  $\tilde{\mathbf{h}}_{j,r,b}^T = [(\text{diag}(\mathbf{h}_{r,b}^H) \mathbf{h}_{p_j,r})^T \ h_{j,b}]$ , and  $\tilde{\Phi}_{j,b} = \tilde{\mathbf{h}}_{j,r,b} \tilde{\mathbf{h}}_{j,r,b}^H$ .  $\hat{\mathbf{H}}_s$  and  $\hat{\mathbf{H}}_{s,j}$  are shown as

$$\hat{\mathbf{H}}_s = \begin{pmatrix} \text{diag}(\mathbf{h}_{r,b}^H) \mathbf{H}_{s,r} \\ \mathbf{h}_s^H \end{pmatrix},$$

$$\hat{\mathbf{H}}_{s,j} = \begin{pmatrix} \text{diag}(\mathbf{h}_{r,j}^H) \mathbf{H}_{s,r} \\ \mathbf{h}_{s,j}^H \end{pmatrix}.$$

P0 is non-convex for jointly optimizing  $\mathbf{v}_s$  and  $\hat{\boldsymbol{\theta}}$  because of the coupling between  $\mathbf{v}_s$  and  $\hat{\boldsymbol{\theta}}$  in the objective function (13a) and the constraints (13b). This brings a big challenge to search the optimal beamforming vector and reflecting coefficients jointly. In fact, even with  $\mathbf{v}_s$  fixed, the optimization on  $\hat{\boldsymbol{\theta}}$  in P0 is still non-convex. Since  $\hat{\mathbf{H}}_s \mathbf{v}_s \mathbf{v}_s^H \hat{\mathbf{H}}_s^H \succeq 0$  and  $\sum_{j=1}^J P_j \tilde{\Phi}_{j,b} \succeq 0$ , the numerator and denominator in the SIR of P0 are convex functions of  $\hat{\boldsymbol{\theta}}$ . Although the domain of  $\hat{\boldsymbol{\theta}}$  with the constraints in P0 is a compact convex set by fixing  $\mathbf{v}_s$ , the fractional programming of the SIR in P0 on  $\hat{\boldsymbol{\theta}}$  is convex-concave, which also results in the non-concave property.

### III. ALTERNATIVE OPTIMIZATION ON BEAMFORMING VECTOR AND THE REFLECTING COEFFICIENTS

Since the non-concave property of the P0 causes the difficulty to obtain the optimal solution by optimizing beamforming vector and the reflecting coefficients jointly, we propose to optimize  $\mathbf{v}_s$  and  $\hat{\boldsymbol{\theta}}$  in P0 alternatively for the sub-optimal objective value. Although the thought of AO method is intuitional, the methods to optimize  $\mathbf{v}_s$  and  $\hat{\boldsymbol{\theta}}$  need to be investigated with the characteristics of each subproblem, respectively. Actually, the maximization of the achievable rate in P0 is equivalent to maximize the SIR in P0. It can be split into two subproblems (P1 and P2) to utilize AO, which are shown as

$$\text{P1: } \max_{\mathbf{v}_s} \frac{\|\hat{\boldsymbol{\theta}}^H \hat{\mathbf{H}}_s \mathbf{v}_s\|^2}{\hat{\boldsymbol{\theta}}^H \left( \sum_{j=1}^J P_j \tilde{\Phi}_{j,b} \right) \hat{\boldsymbol{\theta}}} \quad (14)$$

$$\text{s.t. } (13b) \text{ and } (13e),$$

and

$$\begin{aligned} \text{P2: } \max_{\hat{\boldsymbol{\theta}}} & \frac{\hat{\boldsymbol{\theta}}^H (\hat{\mathbf{H}}_s \mathbf{v}_s \mathbf{v}_s^H \hat{\mathbf{H}}_s^H) \hat{\boldsymbol{\theta}}}{\hat{\boldsymbol{\theta}}^H \left( \sum_{j=1}^J P_j \tilde{\boldsymbol{\Phi}}_{j,b} \right) \hat{\boldsymbol{\theta}}} \\ \text{s.t. } & (13\text{b}), (13\text{c}) \text{ and } (13\text{d}). \end{aligned} \quad (15)$$

In the subsections below, we analyse the solutions of P1 and P2, respectively. In the first subsection, the optimization on beamforming vector in the SOP would be investigated. Then, the optimal DES algorithm for optimizing the reflecting coefficients in the CQFP is illustrated. Besides, the sub-optimal GLD algorithm would also be proposed for the CQFP to reduce the computation overhead.

#### A. The Design of the Optimal Beamforming Vector at the S-AP

With the variable  $\hat{\boldsymbol{\theta}}$  fixed in P1, the SIR in P0 is optimized with the beamforming vector  $\mathbf{v}_s$  of S-AP in P1. Since the value of objective function in P1 remains the same with  $\mathbf{v}_s$  replaced by  $e^{i\phi} \mathbf{v}_s$  ( $\forall \phi \in [0, 2\pi)$ ), P1 is equivalent to P3 shown as

$$\begin{aligned} \text{P3: } \max_{\mathbf{v}_s} & \frac{\text{Re} \left( \hat{\boldsymbol{\theta}}^H \hat{\mathbf{H}}_s \mathbf{v}_s \right)}{\hat{\boldsymbol{\theta}}^H \left( \sum_{j=1}^J P_j \tilde{\boldsymbol{\Phi}}_{j,b} \right) \hat{\boldsymbol{\theta}}} \\ \text{s.t. } & (13\text{b}), (13\text{e}) \text{ and } \text{Im}(\hat{\boldsymbol{\theta}}^H \hat{\mathbf{H}}_s \mathbf{v}_s) = 0, \end{aligned} \quad (16)$$

where  $\text{Re}(\cdot)$  and  $\text{Im}(\cdot)$  denote the real part and the imaginary part of a scalar, a vector or a matrix, respectively.

For the constraints of  $\mathbf{v}_s$  in P3, the feasible domain of  $\mathbf{v}_s$  is a convex set. Besides,  $\mathbf{v}_s$  in (16) is a concave function with known  $\hat{\boldsymbol{\theta}}$ . This implies that P3 can be verified as the maximization of a concave function on  $\mathbf{v}_s$  with the form of second-order cone programming (SOCP) [27], which can be solved with the common algorithms of convex optimization (such as interior point method). Therefore, the optimizing on the beamforming vector at the S-AP in the AO can obtain the optimal solution with the reflecting coefficients fixed.

*B. The Proposed Domain and Envelope Shrinking Algorithm for the Optimal Solution of Reflecting Coefficients at the RIS*

Although  $\mathbf{v}_s$  is fixed in P2, it is still a non-concave problem because of the fractional programming in the objective function with the variable  $\hat{\boldsymbol{\theta}}$ . In this paper, an optimal DES algorithm is proposed to solve P2. Note that P2 can be expressed as an example of P4 (the general form of fractional programming with convex quadratic numerator and denominator).

$$\text{P4: } \max_{\hat{\boldsymbol{\theta}}} \frac{\hat{\boldsymbol{\theta}}^H \mathbf{A} \hat{\boldsymbol{\theta}}}{\hat{\boldsymbol{\theta}}^H \mathbf{B} \hat{\boldsymbol{\theta}}} \quad (17)$$

$$\text{s.t. } \mathbf{A} \succeq 0, \mathbf{B} \succ 0,$$

$$(13\text{b}), (13\text{c}) \text{ and } (13\text{d}).$$

Now, Let us explain the idea of the DES algorithm based on P4. First, the concave envelope of the objective function in P4 is utilized as the upper bound in the iteration of the proposed DES, which would converge to the optimal value of P4. Let us denote the eigenvalue decomposition of  $\mathbf{A}$  by  $\mathbf{W}\boldsymbol{\Psi}\mathbf{W}^H$  with  $\boldsymbol{\Psi} = \text{diag}([\psi_1, \dots, \psi_{N+1}])$ . Then, P4 can be reformulated with the new variable  $\mathbf{u} \triangleq [u_1, u_2, \dots, u_{N+1}]^T = \mathbf{W}^H \hat{\boldsymbol{\theta}}$  and  $\mathbf{t} = [t_1, t_2, \dots, t_{N+1}]^T$  as

$$\text{P5: } \max_{\mathbf{u}, \mathbf{t}} f(\mathbf{u}, \mathbf{t}) = \sum_{n=1}^{N+1} \frac{\psi_n |u_n|^2}{t_n} \quad (18\text{a})$$

$$\text{s.t. } \mathbf{u}^H \mathbf{W}^H \mathbf{B} \mathbf{W} \mathbf{u} = g(\mathbf{u}) \leq t, \quad (18\text{b})$$

$$|\mathbf{W}^H \mathbf{u}^H \hat{\mathbf{H}}_{s,j} \mathbf{v}_s|^2 \leq \bar{\Gamma}_j, \quad j \in \mathcal{J}, \quad (18\text{c})$$

$$|[\mathbf{W} \mathbf{u}]_n| \leq 1, \quad n \in \mathcal{N}, \quad (18\text{d})$$

$$[\mathbf{W} \mathbf{u}]_{N+1} = 1, \quad (18\text{e})$$

$$t_n = t, \quad n \in \bar{\mathcal{N}} = \{1, \dots, N+1\}. \quad (18\text{f})$$

Supposing that the convex hull  $S_n$  includes the vertexes  $\{|u_{n,c}|, t_{n,c}\}, c = 1, 2, 3\}$ ,  $\bar{f}(\boldsymbol{\gamma})$  in (19) denotes a concave envelope of  $f(\mathbf{u}, \mathbf{t})$  over  $S$ . A upper bound of P5 can be illustrated as

$$\text{P6: } \max_{\boldsymbol{\gamma}} \bar{f}(\boldsymbol{\gamma}) = \sum_{n=1}^{N+1} \left( \sum_{c=1}^3 \gamma_{n,c} \frac{\psi_n |u_{n,c}|^2}{t_{n,c}} \right) \quad (19)$$

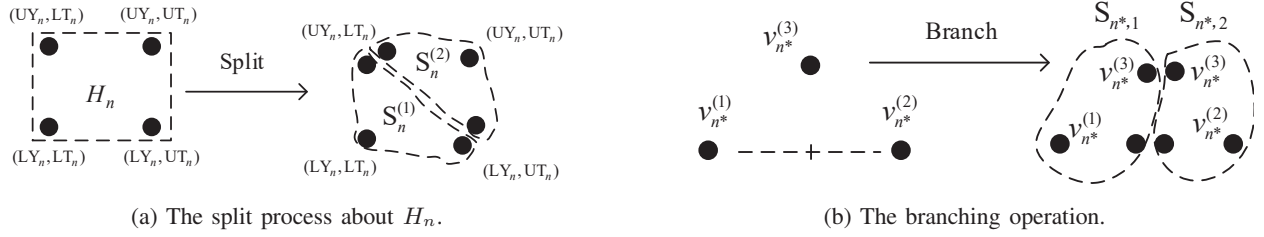


Fig. 2. Some procedures in the DES algorithm.

$$\text{s.t. } \gamma = \{\gamma_{n,c}, n \in \overline{\mathcal{N}}, c = 1, 2, 3\},$$

$$u_n = \sum_{c=1}^3 \gamma_{n,c} u_{n,c}, \quad n \in \overline{\mathcal{N}},$$

$$t_n = \sum_{c=1}^3 \gamma_{n,c} t_{n,c}, \quad n \in \overline{\mathcal{N}},$$

$$\sum_{c=1}^3 \gamma_{n,c} = 1, \quad n \in \overline{\mathcal{N}},$$

$$\sum_{c=1}^3 \gamma_{n,c} \geq 0, \quad n \in \overline{\mathcal{N}},$$

where  $S$  represents a Cartesian product of  $\{S_n, n \in \overline{\mathcal{N}}\}$ , i.e.,  $S = S_1 \times S_2 \cdots \times S_{N+1}$ . Note that  $\bar{f}(\gamma)$  in P6 is unique affine transforming of the set  $\{\psi_n | u_{n,c}|^2/t_{n,c}, n \in \overline{\mathcal{N}}, c = 1, 2, 3\}$ .

The principles about the proposed DES algorithm are based on splitting the domain of the variables of P5 into small polyhedral fragments while decreasing the maximum value ( $\beta_k$ ) of all the valid concave envelopes in P6 in the process of  $k$ -th iteration, where  $k < T$  and  $T$  is maximum number of the iterations in the DES. When the maximum value ( $\alpha_k$ ) of P5 over the sampling points on the grids of valid polyhedral fragments equals  $\beta_k$ , the proposed DES algorithm converges to the optimal value for P4.

In the initialization, the hyperrectangle  $H = H_1 \times H_2 \cdots \times H_{N+1}$  is defined with the Cartesian product of  $H_n = \{(|u_n|, t_n) \in \mathfrak{R}_+^2 | LY_n \leq |u_n| \leq UY_n, LT_n \leq t_n \leq UT_n\}, n \in \overline{\mathcal{N}}$ .  $LY_n$ ,  $UY_n$ ,  $LT_n$  and  $UT_n$  can be obtained by solving  $LY_n = \min |u_n|$ ,  $UY_n = \max |u_n|$ ,  $LT_n = \min g(\mathbf{u})$  and  $UT_n = \max g(\mathbf{u})$  with the same constraints (18c), (18d), and (18e), respectively.

As Fig. 2(a) shows, the  $n$ -th dimension  $H_n$  in  $H$  can be split into two convex hulls  $S_n^{(1)}$  and  $S_n^{(2)}$  based on the partition of the vertexes, shown as  $\{(LY_n, UT_n), (LY_n, LT_n), (UY_n, LT_n)\} \subseteq S_n^{(1)}$  and  $\{(LY_n, UT_n), (UY_n, UT_n), (UY_n, LT_n)\} \subseteq S_n^{(2)}$ . Define the set  $\bar{P}^0 = \{S | S = S_1 \times S_2 \cdots \times S_{N+1}, S_n = S_n^{(1)} \text{ or } S_n^{(2)}, n \in \overline{\mathcal{N}}\}$  where  $S$  is a subset of  $H$  with polyhedral partition, and  $\bar{P}^0$

is the set of polyhedral partition elements for  $H$ . The procedures of the proposed DES for P4 are shown as **Algorithm 1**.

As Fig. 2(b) shows, the branching operation in **Algorithm 1** for any  $S$  can be described as follows. Assume that the vertex set of  $S_n$  is given by  $\{v_n^{(1)}, v_n^{(2)}, v_n^{(3)}\}$  and the longest edge of  $S_n$  denotes the edge connecting  $v_n^{(1)}$  and  $v_n^{(2)}$ , the selected index of branching is defined as  $n^* = \operatorname{argmax}_{n \in \mathcal{N}} \|v_n^{(1)} - v_n^{(2)}\|$ . Then,  $S$  can be subdivided into two new polyhedral partition elements  $\bar{S}^{(1)}$  and  $\bar{S}^{(2)}$  given by  $\bar{S}^{(1)} = S_1 \times \cdots \times S_{n^*-1} \times S_{n^*,1} \times S_{n^*+1} \times \cdots \times S_{N+1}$  and  $\bar{S}^{(2)} = S_1 \times \cdots \times S_{n^*-1} \times S_{n^*,2} \times S_{n^*+1} \times \cdots \times S_{N+1}$ , where  $S_{n^*,1}$  and  $S_{n^*,2}$  are the results from the simplicial bisection of  $S_{n^*}$  on the longest edge.

When  $\beta_k$  and  $\alpha_k$  converge to the same value, the optimal solution of P2 can be confirmed by DES. It is valuable to note that along with the convergence of  $\beta_k$  and  $\alpha_k$ , these values obtained in each iteration provide the upper bound and effective approximation of the optimal value, respectively. This brings useful reference for designing and evaluating low-complexity and heuristic algorithms to find sub-optimal reflecting coefficients.

### C. The Proposed Sub-optimal Method of Gradient-based Linearization with Domain

In the design of the algorithm for CQFP, the computation complexity is important for the application in the practical system. To solve P2 in low complexity, the sub-optimal GLD is proposed to optimize the reflecting coefficients at the RIS. The general idea of GLD can be described as follows. In the beginning, P2 would be transformed as the minimization of a concave function. Then, linearization with domain would be utilized to obtain the local-optimal solution for the minimization of a concave problem, which is a sub-optimal solution for P2.

The problem P2 can be transformed into P7 equivalently, which is the minimization of a concave problem, shown as

$$\text{P7: } \min_{\hat{\boldsymbol{\theta}}, t} \quad -\frac{\|(\hat{\mathbf{H}}_s \mathbf{v}_s)^H \hat{\boldsymbol{\theta}}\|^2}{t} \quad (20a)$$

$$\text{s.t.} \quad \hat{\boldsymbol{\theta}}^H \left( \sum_{j=1}^U P_j \tilde{\boldsymbol{\Phi}}_{j,b} \right) \hat{\boldsymbol{\theta}} \leq t, \quad (20b)$$

$$(13b), (13c), \text{ and } (13d).$$

The equivalence between P2 and P7 can be proven as follows.

---

**Algorithm 1** The Domain and Envelope Shrinking Algorithm for P4
 

---

- 1: **Initial:** set the maximum number of iterations  $T$ ,  $P^0 \leftarrow \emptyset$ ,  $\alpha_0 \leftarrow -\infty$ .
  - 2: **for**  $\forall S \in \bar{P}^0$  **do**
  - 3:   the optimal value  $\text{UB}(S)$  of convex programming in P6 exists with the parameters  $(\mathbf{u}^S, \mathbf{t}^S)$ .
  - 4:    $\alpha_0 \leftarrow \max\{\alpha_0, f(\mathbf{u}^S, \mathbf{t}^S)\}$  in P5,  $(\mathbf{u}^0, \mathbf{t}^0)$  is the solution for  $\alpha_0 = f(\mathbf{u}^0, \mathbf{t}^0)$ .
  - 5:   **if**  $\text{UB}(S) > \alpha_0$  **then**
  - 6:      $P^0 \leftarrow P^0 \cup \{S\}$
  - 7:   **end if**
  - 8: **end for**
  - 9: **if**  $P^0 = \emptyset$  **then**
  - 10:    $I_{\text{run}} \leftarrow 0$ , stop,  $(\mathbf{u}^0, \mathbf{t}^0)$  is the optimal solution for P5.
  - 11: **else**
  - 12:    $\beta_0 \leftarrow \max\{\text{UB}(S) | S \in P^0\}$ ,  $I_{\text{run}} \leftarrow 1$ .
  - 13: **end if**
  - 14:  $k \leftarrow 0$
  - 15: **while**  $\beta_k - \alpha_k > 0 \& I_{\text{run}} = 1 \& k < T$  **do**
  - 16:    $k \leftarrow k + 1$ , remove the element  $S$  from  $P^{k-1}$  when  $\text{UB}(S) \leq \alpha_{k-1}$ .
  - 17:   Define  $\Xi_S = \{S \in P^{k-1}, \text{UB}(S) = \beta_{k-1}\}$ , Each  $S$  in  $\Xi_S$  is split into  $\{\bar{S}^{(1)}, \bar{S}^{(2)}\}$  added into  $P_0^k$  with the branching operation.
  - 18:   remove the elements in  $P_0^k$  if the elements are infeasible for P5.
  - 19:    $\forall S \in P_0^k$ , obtain the optimal value  $\text{UB}(S)$  and the corresponding parameters  $(\mathbf{u}^S, \mathbf{t}^S)$  for P6.  $\alpha_k \leftarrow \max\{\alpha_{k-1}, \max\{f(\mathbf{u}^S, \mathbf{t}^S) | S \in P_0^k\}\}$  and  $\alpha_k = f(\mathbf{u}^k, \mathbf{t}^k)$ .
  - 20:    $P^k \leftarrow (P^{k-1} \setminus \Xi_S) \cup P_0^k$ ,  $\beta_k \leftarrow \max\{\text{UB}(S) | S \in P^k\}$ .
  - 21: **end while**
  - 22: **if**  $\beta_k - \alpha_k = 0$  **then**
  - 23:    $(\mathbf{u}^k, \mathbf{t}^k)$  is the optimal solution for P5,  $\beta_T \leftarrow \beta_k$ ,  $\alpha_T \leftarrow \alpha_k$ .
  - 24: **else**
  - 25:    $\beta_T$  and  $\alpha_T$  can be the upper bound and the lower bound for the objective value of P5.
  - 26: **end if**
-

*Proof:* If  $\hat{\boldsymbol{\theta}}_0$  is the optimal solution for P2, define  $t_0 = \hat{\boldsymbol{\theta}}_0^H (\sum_{j=1}^U P_j \tilde{\boldsymbol{\Phi}}_{j,b}) \hat{\boldsymbol{\theta}}_0$ . Then,  $(\hat{\boldsymbol{\theta}}_0, t_0)$  is a feasible solution for P7. Assuming  $(\hat{\boldsymbol{\theta}}_0, t_0)$  is not the optimal solution for P7, the optimal solution  $(\hat{\boldsymbol{\theta}}_1, t_1)$  of P7 exists and  $\|(\hat{\mathbf{H}}_s \mathbf{v}_s)^H \hat{\boldsymbol{\theta}}_1\|^2 / t_1 > \|(\hat{\mathbf{H}}_s \mathbf{v}_s)^H \hat{\boldsymbol{\theta}}_0\|^2 / t_0$ . Therefore,

$$\frac{\|(\hat{\mathbf{H}}_s \mathbf{v}_s)^H \hat{\boldsymbol{\theta}}_1\|^2}{\hat{\boldsymbol{\theta}}_1^H (\sum_{j=1}^J P_j \tilde{\boldsymbol{\Phi}}_{j,b}) \hat{\boldsymbol{\theta}}_1} \geq \frac{\|(\hat{\mathbf{H}}_s \mathbf{v}_s)^H \hat{\boldsymbol{\theta}}_1\|^2}{t_1} > \frac{\|(\hat{\mathbf{H}}_s \mathbf{v}_s)^H \hat{\boldsymbol{\theta}}_0\|^2}{\hat{\boldsymbol{\theta}}_0^H (\sum_{j=1}^J P_j \tilde{\boldsymbol{\Phi}}_{j,b}) \hat{\boldsymbol{\theta}}_0}$$

exists, which means that  $\hat{\boldsymbol{\theta}}_1$  is a feasible solution for P2 with higher value for objective function of P2, compared with the optimal solution  $\hat{\boldsymbol{\theta}}_0$  for P2. This results in the contradiction with the definition of  $\hat{\boldsymbol{\theta}}_0$  for P2. Therefore,  $(\hat{\boldsymbol{\theta}}_0, t_0)$  is also an optimal solution for P7.

If  $(\hat{\boldsymbol{\theta}}_2, t_2)$  is the optimal solution for P7,  $t_2 = \hat{\boldsymbol{\theta}}_2^H (\sum_{j=1}^U P_j \tilde{\boldsymbol{\Phi}}_{j,b}) \hat{\boldsymbol{\theta}}_2$  can be proven. The explanation is illustrated as follows. If  $t_2 \neq \hat{\boldsymbol{\theta}}_2^H (\sum_{j=1}^U P_j \tilde{\boldsymbol{\Phi}}_{j,b}) \hat{\boldsymbol{\theta}}_2$ ,  $t_2 > \hat{\boldsymbol{\theta}}_2^H (\sum_{j=1}^U P_j \tilde{\boldsymbol{\Phi}}_{j,b}) \hat{\boldsymbol{\theta}}_2$  is obtained with the constraints (20b). Then, a smaller value for objective function of P7 with solution  $(\hat{\boldsymbol{\theta}}_2, \hat{t}_2)$  is obtained, where  $\hat{t}_2 = \hat{\boldsymbol{\theta}}_2^H (\sum_{j=1}^U P_j \tilde{\boldsymbol{\Phi}}_{j,b}) \hat{\boldsymbol{\theta}}_2$ . This also results in the contradiction with the definition of  $(\hat{\boldsymbol{\theta}}_2, t_2)$  for P7. With  $t_2 = \hat{\boldsymbol{\theta}}_2^H (\sum_{j=1}^U P_j \tilde{\boldsymbol{\Phi}}_{j,b}) \hat{\boldsymbol{\theta}}_2$ ,  $\hat{\boldsymbol{\theta}}_2$  is the optimal solution for P7' shown as

$$\begin{aligned} \text{P7'} : \quad & \min_{\hat{\boldsymbol{\theta}}, t} \quad - \frac{\|(\hat{\mathbf{H}}_s \mathbf{v}_s)^H \hat{\boldsymbol{\theta}}\|^2}{t} & (21) \\ & \text{s.t.} \quad \hat{\boldsymbol{\theta}}^H \left( \sum_{j=1}^U P_j \tilde{\boldsymbol{\Phi}}_{j,b} \right) \hat{\boldsymbol{\theta}} = t, \\ & (13b), (13c), \text{ and } (13d). \end{aligned}$$

The equivalence between P2 and P7' is obvious. With all the derivations and illustrations shown, P2 is equivalent to P7. ■

Since the function  $f(\mathbf{x}, t) = \|\mathbf{x}\|^2/t$  is convex over  $(\mathbf{x}, t \in \mathfrak{R}_+)$ ,  $q(\hat{\boldsymbol{\theta}}, t) \triangleq -\|(\hat{\mathbf{H}}_s \mathbf{v}_s)^H \hat{\boldsymbol{\theta}}\|^2/t$  is concave over  $(\hat{\boldsymbol{\theta}}, t \in \mathfrak{R}_+)$ . As P7 is the minimization over the concave problem, the common methods in convex optimization to solve the minimization over a convex function for the optimal solution could not be utilized. However, the approximation of the concave objective function in P7 with linearization can be considered to obtain a sub-optimal solution for P7. Linear approximation is the variation of Taylor expansion by cutting off the Lagrange form of the remainder or the Peano form of the remainder, which is in second order. Therefore, the value of the linear approximation for the objective function in P7 is higher than the optimal value in P7 for the convexity of the function  $\|\mathbf{x}\|^2/t$ , which can explain the sub-optimality of GLD.

With  $\varpi^T = [\hat{\boldsymbol{\theta}}^T \ t]$  defined, linearization is utilized to make  $q(\varpi)$  convexified on  $\varpi_k$  as

$$\hat{q}(\varpi; \varpi_k) \triangleq q(\varpi_k) + \nabla q(\varpi_k)^T (\varpi - \varpi_k), \quad (22)$$

where  $\hat{q}(\varpi; \varpi_k)$  is an affine function with convexity and  $k$  is the count number of the iteration in the GLD. The domain of  $\varpi$  is  $\mathcal{D}$  determined by the constraints (13b), (13c), (13d) and (20b), and the convexity of the domain can be easily validated.

To keep any feasible point for the problem (22) in  $\mathcal{D}$ , the penalty item should be added in (22) for the points out of  $\mathcal{D}$ . The linearization for P7 with domain is shown as

$$\begin{aligned} \tilde{q}(\varpi; z) &\triangleq q(z) + \nabla q(z)^T (\varpi - z) + \mathcal{I}(\varpi), \\ \mathcal{I}(\varpi) &\triangleq \begin{cases} 0 & \varpi \in \mathcal{D}, \\ \infty & \varpi \notin \mathcal{D}. \end{cases} \end{aligned} \quad (23)$$

Since  $\mathcal{I}(\varpi)$  is a convex function and (22) is an affine function,  $\tilde{q}(\varpi; z)$  in (23) is convex. The gradient of  $q(\varpi)$  can be obtained as

$$\nabla q(\varpi)^T = [-\hat{\boldsymbol{\theta}}^H (\hat{\mathbf{H}}_s \mathbf{v}_s \mathbf{v}_s^H \hat{\mathbf{H}}_s^H) / t \quad \|(\hat{\mathbf{H}}_s \mathbf{v}_s)^H \hat{\boldsymbol{\theta}}\|^2 / t^2]. \quad (24)$$

Since the optimization of (22) includes the process of iteration for  $\varpi_k$ ,  $\varpi_k$  may be on the boundary of the  $\mathcal{D}$ . Therefore, the convex function  $\hat{q}(\varpi; \varpi_k)$  may not be differentiable at  $\varpi_k$ . If  $\bar{\varpi}_k$  in  $q(\bar{\varpi}_k)$  is on the boundary of  $\mathcal{D}$ , the damped process as  $\varpi_k = \varepsilon \bar{\varpi}_k + (1 - \varepsilon) \varpi_{k-1}$  is executed with  $\varepsilon \in (0, 1)$ . If  $\varpi_0$  is in the interior of  $\mathcal{D}$ ,  $\varpi_k$  will be guaranteed in the interior of  $\mathcal{D}$ .

In the initial phase, the GLD attempts to obtain a feasible solution for P7 randomly. With this feasible point in the domain of P7, the objective function in P7 would be approximated by a line segment with the linearization operation. The optimal solution for the line segment in the feasible domain of P7 is solved as the updated feasible point to start next iteration. Therefore, the iteration of the  $\varpi_k$  would converge to a local minimum point of the objective function in P7, which is a sub-optimal solution of the reflecting coefficients at the RIS. In summary, the GLD algorithm is shown as **Algorithm 2**.

#### IV. THE PRACTICAL CONSIDERATIONS FOR THE RIS-AIDED SSS WITH MULTIPLE PRIMARY NETWORKS

In the practical RIS-aided SSS with multiple primary networks, there are some issues to be considered, which are corresponding to the cost of building the system and the economic reward.

---

**Algorithm 2** The Gradient-based Linearization with Domain algorithm for P7

---

- 1: Initial: given  $\varpi_0$  in interior of  $\mathcal{D}$  randomly,  $\tau_0 = q(\varpi_0)$ ,  $\tau_{-1} = -\infty$ .
  - 2:  $k \leftarrow 0$
  - 3: **while**  $\tau_k > \tau_{k-1}$  **do**
  - 4:   Linearization with domain:  $\tilde{q}(\varpi; \varpi_k) = q(\varpi_k) + \nabla q(\varpi_k)^T(\varpi - \varpi_k) + \mathcal{I}(\varpi)$ .
  - 5:   Solve the convex subproblem with interior point method: obtain the solution  $\bar{\varpi}_{k+1}$  for  $\tau_k = \min_{\varpi} \tilde{q}(\varpi; \varpi_k)$  with the constraints (13b), (13c), (13d) and (20b).
  - 6:   **if**  $\bar{\varpi}_{k+1}$  is in the interior of  $\mathcal{D}$  **then**
  - 7:      $\varpi_{k+1} \leftarrow \bar{\varpi}_{k+1}$
  - 8:   **else**
  - 9:      $\varpi_{k+1} \leftarrow \varepsilon \bar{\varpi}_k + (1 - \varepsilon)\varpi_k$ ,  $\varepsilon \in (0, 1)$ .
  - 10:   **end if**
  - 11:    $k \leftarrow k + 1$
  - 12: **end while**
- 

For example, the budget on the power expense for the operator depends on the EE performance of the system. Besides, the discretization of the reflecting coefficients on the RIS can elevate the feasibility of the RIS deployment in the SSS with multiple primary networks.

*A. The Energy Efficiency of RIS-aided Spectrum Sharing System with Multiple Primary Networks*

Since RIS is a low-cost device by reflecting the signal passively, the involving of RIS in the SSS with multiple primary networks would improve the EE of the secondary network significantly. Compared with the SSS without RIS, the RIS-aided SSS can obtain the enhancement on the SE with limited power consumption for enabling the RIS in working mode.

Usually, the total power consumption of the secondary network in RIS-aided SSS includes the transmit power of the S-AP ( $p_s$ ), the static circuit power consumption of the S-AP and the SU ( $P_{S-AP}$  and  $P_{SU}$ ), and the power consumption of the RIS. The EE performance of the RIS-aided secondary network can be denoted as

$$\eta_{\text{ris}} = \frac{\log_2 \left( 1 + \frac{\hat{\boldsymbol{\theta}}^H (\hat{\mathbf{H}}_s \mathbf{v}_s \mathbf{v}_s^H \hat{\mathbf{H}}_s^H) \hat{\boldsymbol{\theta}}}{\hat{\boldsymbol{\theta}}^H (\sum_{j=1}^J P_j \hat{\boldsymbol{\Phi}}_{j,b}) \hat{\boldsymbol{\theta}}} \right)}{p_s + P_{S-AP} + P_{SU} + NP_{\text{eris}}}, \quad (25)$$

where  $P_{\text{eris}}$  denotes the power consumption of each element on the RIS. Correspondingly, the EE performance of the secondary network without RIS is also presented as

$$\eta_0 = \frac{\log_2 \left( 1 + \|\mathbf{h}_s^H \mathbf{v}_s\|^2 / \sigma_{z_b}^2 \right)}{p_s + P_{\text{S-AP}} + P_{\text{SU}}}. \quad (26)$$

Assuming  $\nu$  is the power amplifier efficiency of the S-AP,  $p_s = \mathbf{v}_s^H \mathbf{v}_s / \nu$  is obtained. Although the power consumption of the RIS increases with  $N$ ,  $\eta_{\text{ris}}$  can be improved with the significant gain of the SE in the RIS-aided SSS with multiple PNs.

As (25) is shown, if the number of the elements on the RIS  $N$  is fixed, the power in the denominator of (25) is consumed mostly by static supporting power of the S-AP, the SU and RIS. Therefore, the EE performance can be homogeneously optimized by improving the achievable rate of the SU. Compared with the SSS without RIS, the proposed GLD method can also provide higher EE performance for the RIS-aided SSS. Moreover, the EE performance of the SSS without the RIS in (26) is determined by the permitted transmit power of the S-AP or the beamforming vector at the S-AP.

### B. The Discretization of the Reflecting Coefficients on the RIS

Although the amplitudes and phase shifts of reflecting coefficients at the RIS in P0 are continuous variables ranging in  $[0, 1]$  and  $[0, 2\pi)$  respectively, the amplitudes and phase shifts in practical system about the RIS are selected from discrete values for the characteristics of the RIS devices. Usually, the amplitudes can be zero or one, while the phase shifts can be quantified by 1 bit or 2 bits [25].

If the phase shifts of  $\hat{\boldsymbol{\theta}}$  in P0 are discrete variables, P0 will become a mixed integer non-linear problem (MINLP), which is more complicated to be solved. The discrete phase shifts of  $\hat{\boldsymbol{\theta}}$  can be relaxed to continuous variables to obtain the solution, which is corresponding to P0. Then, the continuous solution can be quantified to discrete phase shifts. However, the new solution should be feasible for the constraints (13b) and decrease the deterioration of SE performance for the discretization of phase shifts. Assuming that  $\bar{\boldsymbol{\theta}}$  is a continuous solution for P0 and there are  $L$  levels ( $\{\phi_1, \dots, \phi_L\}$ ) for the quantization of phase shifts, the quantization problem about the phase shifts of the reflecting coefficients can be illustrated as

$$\text{P8: } \min_{\boldsymbol{\theta}_d} \|\bar{\boldsymbol{\theta}} - \boldsymbol{\theta}_d\|^2 \quad (27a)$$

$$\text{s.t. } \angle([\boldsymbol{\theta}_d]_n) \in \{\phi_1, \dots, \phi_L\}, n \in \mathcal{N}, \quad (27b)$$

$$|\boldsymbol{\theta}_d^H \hat{\mathbf{H}}_{s,j} \mathbf{v}_s|^2 \leq \bar{\Gamma}_j, j \in \mathcal{J}. \quad (27c)$$

For a small number of reflecting coefficients, the exhaustive searching method can be utilized to obtain the discrete solution of  $\boldsymbol{\theta}_d$ , which should conform to the constraints of (13b) and optimize the objective function of P0.

In this paper, the NPSP is proposed to obtain the sub-optimal solution about the discrete reflecting coefficients. The NPSP method would focus on searching the nearest point in the candidate set of the discrete value of the phase shifts, where the objective function would be added with the penalty for invalidation of constraints. Let us introduce an auxiliary vector  $\mathbf{b}$  for  $\boldsymbol{\theta}_d$ . Then, the problem about NPSP for solving discrete phase shifts of the reflecting coefficients at the RIS is formulated as

$$\text{P9: } \min_{\boldsymbol{\theta}_d, \mathbf{b}} \quad \|\bar{\boldsymbol{\theta}} - \mathbf{b}\|^2 + \frac{\mu}{2} \|\mathbf{b} - \boldsymbol{\theta}_d\| \quad (28a)$$

$$\text{s.t. } \mathbf{b} = \boldsymbol{\theta}_d, \quad (28b)$$

$$(27b) \text{ and } (27c),$$

where  $\mu > 0$  is the penalty parameters. Given the Lagrange variables  $\mathbf{w} = [w_1, \dots, w_J]^T \succeq 0$  and  $\boldsymbol{\lambda} = \boldsymbol{\lambda}_R + i\boldsymbol{\lambda}_I$  ( $\boldsymbol{\lambda}_R = [\lambda_{R,1}, \dots, \lambda_{R,N}]^T$  and  $\boldsymbol{\lambda}_I = [\lambda_{I,1}, \dots, \lambda_{I,N}]^T$ ) for  $\text{Re}\{\mathbf{b} - \boldsymbol{\theta}_d\} = 0$  and  $\text{Im}\{\mathbf{b} - \boldsymbol{\theta}_d\} = 0$ , the Lagrangian function for P9 is

$$\begin{aligned} \mathcal{G}(\mathbf{b}, \boldsymbol{\theta}_d, \boldsymbol{\lambda}, \mathbf{w}) = & (\mathbf{b} - \bar{\boldsymbol{\theta}})^H (\mathbf{b} - \bar{\boldsymbol{\theta}}) + \frac{\mu}{2} (\mathbf{b} - \boldsymbol{\theta}_d)^H (\mathbf{b} - \boldsymbol{\theta}_d) \\ & + \sum_{n=1}^N \mathcal{I}_n([\boldsymbol{\theta}_d]_n) + \text{Re}\{\boldsymbol{\lambda}^H (\mathbf{b} - \boldsymbol{\theta}_d)\} \\ & + \sum_{j=1}^J w_j (|\boldsymbol{\theta}_d^H \hat{\mathbf{H}}_{s,j} \mathbf{v}_s|^2 - \bar{\Gamma}_j), \end{aligned} \quad (29)$$

where  $\mathcal{I}_n(\cdot)$  is the indicator function ( $\mathcal{I}_n(x) = 1$  if  $x \in \{[|\bar{\boldsymbol{\theta}}]_n|e^{i\phi_1}, \dots, [|\bar{\boldsymbol{\theta}}]_n|e^{i\phi_L}\}$ , otherwise  $+\infty$ ). Then, the dual problem can be defined as

$$\mathcal{L}(\boldsymbol{\lambda}, \mathbf{w}) \triangleq \inf_{\mathbf{b}, \boldsymbol{\theta}_d} \mathcal{G}(\mathbf{b}, \boldsymbol{\theta}_d, \boldsymbol{\lambda}, \mathbf{w}) \quad (30)$$

To solve P9 with the NPSP, the iterations about the parameters are shown as follows.

$$\boldsymbol{\theta}_d^{k+1} = \arg \min_{\boldsymbol{\theta}_d} \mathcal{G}(\mathbf{b}^k, \boldsymbol{\theta}_d, \boldsymbol{\lambda}^k, \mathbf{w}^k), \quad (31a)$$

$$\mathbf{b}^{k+1} = \arg \min_{\mathbf{b}} \mathcal{G}(\mathbf{b}, \boldsymbol{\theta}_d^{k+1}, \boldsymbol{\lambda}^k, \mathbf{w}^k), \quad (31b)$$

$$\boldsymbol{\lambda}^{k+1} = \boldsymbol{\lambda}^k + \mu(\mathbf{b}^{k+1} - \boldsymbol{\theta}_d^{k+1}), \quad (31c)$$

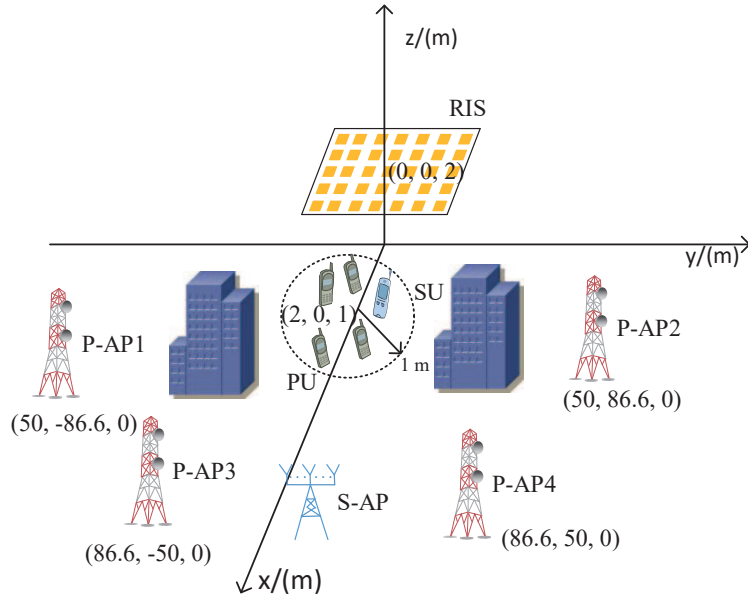


Fig. 3. One secondary network coexisting with multiple primary networks in the simulated scenarios.

$$w_j^{k+1} = w_j^k + \mu(|\boldsymbol{\theta}_d^{k+1} \hat{\mathbf{H}}_{s,j} \mathbf{v}_s|^2 - \bar{\Gamma}_j)^+, j \in \mathcal{J}, \quad (31d)$$

since  $(\mathbf{H}_{s,j} \mathbf{v}_s)^H (\mathbf{H}_{s,j} \mathbf{v}_s)$  is a real number, (32) is obtained for the angle calculation.

$$\angle \left( \frac{\mathbf{b}^k + \boldsymbol{\lambda}^k / \mu}{1 + \sum_{j=1}^J w_j (\mathbf{H}_{s,j} \mathbf{v}_s)^H (\mathbf{H}_{s,j} \mathbf{v}_s)} \right) = \angle (\mathbf{b}^k + \boldsymbol{\lambda}^k / \mu) \quad (32)$$

Therefore,  $\boldsymbol{\theta}_d^{k+1}$  in (31a) can be solved by

$$\begin{aligned} \angle(\boldsymbol{\theta}_d^{k+1}) &\triangleq \arg \min_{\boldsymbol{\varphi}} \|\boldsymbol{\varphi} - \angle(\mathbf{b}^k + \boldsymbol{\lambda}^k / \mu)\|, \\ [\boldsymbol{\varphi}]_n &\in \{\phi_1, \dots, \phi_L\}, \|\boldsymbol{\theta}_d^{k+1}\|_n \triangleq [\bar{\boldsymbol{\theta}}]_n, n \in \mathcal{N}. \end{aligned} \quad (33)$$

Besides,  $\mathbf{b}^{k+1}$  in (31b) can be solved by

$$\mathbf{b}^{k+1} = ((2 + \mu)\mathbf{I}_N + 2\mathbf{Y})^{-1} (2\bar{\boldsymbol{\theta}} + \mu\boldsymbol{\theta}_d^{k+1} + \boldsymbol{\lambda}^{k+1}), \quad (34)$$

where  $\mathbf{Y} = \sum_{j=1}^J w_j^k (\mathbf{H}_{s,j} \mathbf{v}_s) (\mathbf{H}_{s,j} \mathbf{v}_s)^H$ . Then, the proposed NPSP algorithm to solve P9 problem can be shown as **Algorithm 3**.

Since  $\boldsymbol{\theta}_d$  is the discretization of the  $\bar{\boldsymbol{\theta}}$ , the constraints of (27c) may become invalid. Therefore, the feasible  $\boldsymbol{\theta}_d$  may not exist for some CSI  $\mathbf{H}_{s,j}$  and the beamforming vector  $\mathbf{v}_s$ , especially with a small number of elements at the RIS.

---

**Algorithm 3** The Nearest Point Searching with Penalty algorithm for P9
 

---

- 1: Initial: given  $\lambda^0, \mathbf{b}^0, \mathbf{w}^0$  randomly,  $F_{\text{obj}}^0 \leftarrow +\infty$ . Set the terminating threshold  $\varsigma$  for objective function in P8 and  $N_{\text{itr}}$  for maximum number of iteration.
  - 2:  $k \leftarrow 0$
  - 3: **while**  $F_{\text{obj}}^k > \varsigma \& k < N_{\text{itr}}$  **do**
  - 4:   Update  $\theta_{\text{d}}^{k+1}$  and  $\mathbf{b}^{k+1}$  with (33) and (34), respectively
  - 5:   **if**  $\theta_{\text{d}}^{k+1}$  meets the constraints in (27c) **then**
  - 6:     **if**  $\|\bar{\theta} - \theta_{\text{d}}^{k+1}\|^2 < F_{\text{obj}}^k$  **then**
  - 7:        $\theta_{\text{o}} \leftarrow \theta_{\text{d}}^{k+1}$
  - 8:     **end if**
  - 9:      $F_{\text{obj}}^{k+1} \leftarrow \min\{\|\bar{\theta} - \theta_{\text{d}}^{k+1}\|^2, F_{\text{obj}}^k\}$
  - 10:   **end if**
  - 11:   Update  $\lambda^{k+1}$  and  $\mathbf{w}^{k+1}$  with (31c) and (31d), respectively
  - 12:    $k \leftarrow k + 1$
  - 13: **end while**
  - 14: **if**  $F_{\text{obj}}^k = +\infty \& k = N_{\text{itr}}$  **then**
  - 15:   The feasible solution for  $\theta_{\text{d}}$  is not searched.
  - 16: **else**
  - 17:   Output  $\theta_{\text{o}}$
  - 18: **end if**
- 

## V. SIMULATION RESULTS AND DISCUSSIONS

In this section, simulation results are shown to evaluate the performance of RIS-assisted spectrum sharing with multiple primary networks. The number of primary networks ranges from 2 to 4. The general simulation setup is shown in Fig. 3. Specifically, the candidate P-APs are placed uniformly with the distance 100 m to the RIS, respectively. Moreover, the PUs and the SU are distributed randomly in the circular region of x-y plane with the center located at the point (2, 0, 1) m and the radius  $r_u = 1$  m. The path losses of direct link and the cascaded link over the RIS are 106 dB and 123 dB, respectively, which are calculated by following the parameters given in Table I [28] [29]. In particular, due to the double fading effect [5], the path loss of the cascaded link over RIS is larger than that of the direct link.

TABLE I  
THE PARAMETERS OF THE SIMULATION

Parameters	Values
Path loss for RIS-assisted channel	35.6+22.0 lg d
Path loss for direct channel	32.6+36.7 lg d
$P_{\max}$	-2 dBm ~ 14 dBm
$\bar{\Gamma}_j$	-115 dBm, $j \in \mathcal{J}$
$P_j$	10 dBm, $j \in \mathcal{J}$
$P_{S-AP}$	39 dBm
$P_{SU}$	10 dBm
$P_{eris}$	10 dBm

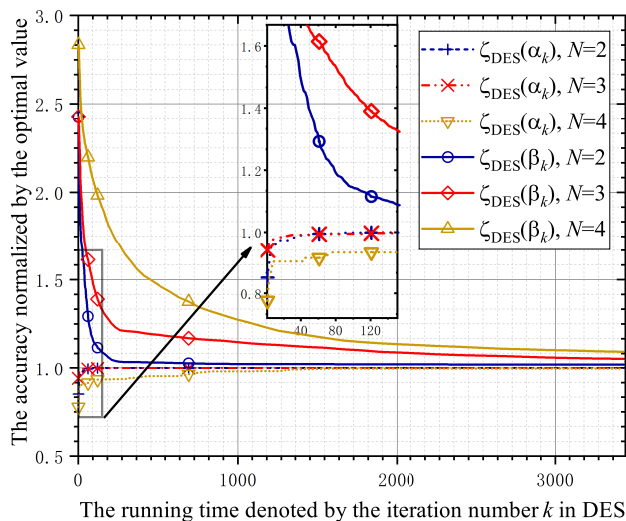


Fig. 4. The convergence situation for  $\beta_k$  of DES and  $\alpha_k$  of DES normalized by the optimal value as the number of the elements of the RIS ranges from 2 to 4<sup>1</sup>.

Fig. 4 shows the convergence situation about the  $\beta_k$  and  $\alpha_k$  normalized by the optimal value for the proposed DES algorithm, denoted by  $\zeta_{DES}(\beta_k)$  and  $\zeta_{DES}(\alpha_k)$ , respectively. As Fig. 4 is shown, the DES in **Algorithm 1** actually provides the ascending sequence of lower bound  $\{\alpha_k\}$  (also sub-optimal values for P2) and the descending sequence of upper bound  $\{\beta_k\}$  for the optimal value of P2. As the number of iterations  $k$  increases in **Algorithm 1**, the optimal value is obtained when  $\beta_k = \alpha_k$ . To verify the optimal solution in DES,  $\zeta_{DES}(\beta_k)$  and  $\zeta_{DES}(\alpha_k)$  should decrease and increase to 1, respectively. The convergence between  $\zeta_{DES}(\beta_T)$  and  $\zeta_{DES}(\alpha_T)$  become slow as  $N$  increases, which indicates that the decreasing of  $\beta_T$  need more running time

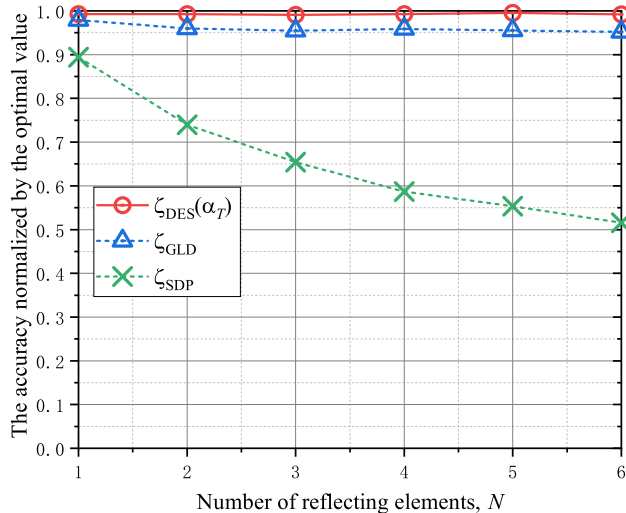


Fig. 5.  $\alpha_T$  of DES, the objective value of GLD and the objective value of SDP for P2 normalized by the optimal value.

for large  $N$ .

Fig. 5 shows the accuracy normalized by the optimal value for the proposed DES algorithm, the proposed sub-optimal GLD method and the compared SDP method [27]. In Fig. 5,  $\alpha_T$  of DES, the objective value of GLD and the objective value of SDP are normalized by the optimal value of P2, denoted by  $\zeta_{DES}(\alpha_T)$ ,  $\zeta_{GLD}$  and  $\zeta_{SDP}$ . As shown in Fig. 5,  $\zeta_{DES}(\alpha_T)$  nearly equals to 1, which means that the lower bound of DES can converge to the optimal value with enough iterations.  $\zeta_{GLD}$  can approximate to  $\zeta_{DES}(\alpha_T)$  with a small gap stably, which explains the effectiveness of the method GLD. On the contrary, since the deterioration of  $\zeta_{SDP}$  is sensitive to  $N$ , the gap between  $\zeta_{DES}(\alpha_T)$  and  $\zeta_{SDP}$  becomes larger as  $N$  increases.

As the GLD possesses a stable effectiveness in low complexity, we can use the proposed GLD algorithm to get a sub-optimal solution with constrained running time. Fig. 6 shows the SE performance of the proposed GLD method with the varying parameter  $N$  of the RIS as the maximum transmit power of the S-AP increases from  $-2$  dBm to  $14$  dBm. Compared with the scenario without RIS in Fig. 6, the system of RIS-assisted spectrum sharing can have obvious gain on the SE performance, even with  $N = 1$ . For the objective function of P2, the increasing on the parameter  $N$  of the RIS not only provide more flexibility on the optimization of the numerator in P2, may also amplify or diminish the denominator in P2. As Fig. 6 shows, our proposed GLD method can improve the objective value in P0, which indicates that the increasing

<sup>1</sup>The optimal value is obtained by exhaustive search, whose running time increase exponentially as  $N$  increases.

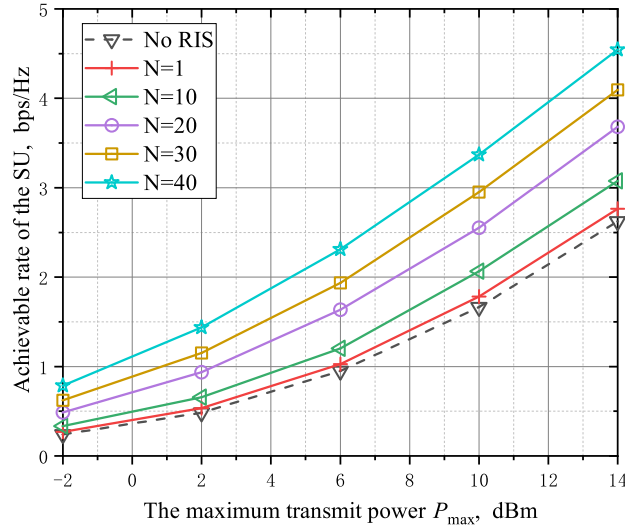


Fig. 6. The achievable rates of the SU realized by the GLD method as  $N$  varies.

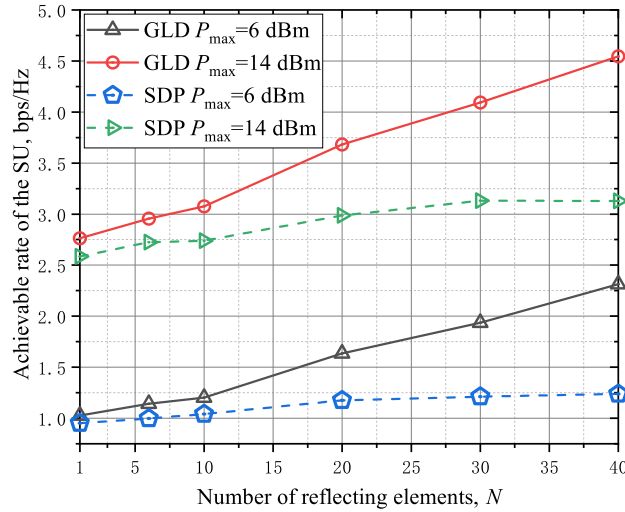


Fig. 7. The achievable rates of the SU obtained by the GLD and the compared SDP as the number of reflecting elements  $N$  increases.

on  $N$  can realize the enhancement on the SE performance of the system. When  $P_{\max}$  ranges in the interval of high power (6 dBm  $\sim$  14 dBm), the proposed GLD method can achieve better SE of the system as  $N$  becomes larger (e.g. over 20 in Fig. 6).

Fig. 7 compares the SE performance of the proposed GLD method with that of the SDP method. As shown in Fig. 7, the achievable rate of the SDP method can approximate to that of the proposed GLD method with a small gap when the number of the elements at the RIS is not so large (e.g. less than 10). Since the numerator is dominant in P1 for a lower  $N$ , the proposed GLD method and the SDP method have the similar performance. When the number

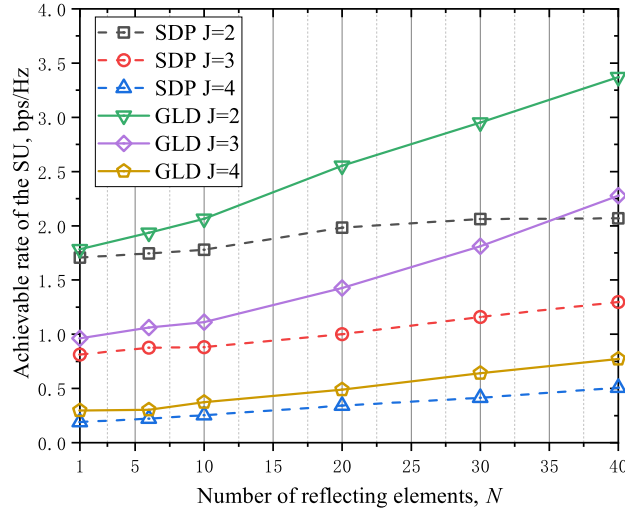


Fig. 8. The achievable rates of the SU obtained by the GLD method and the compared SDP method as the number of primary networks increases from 2 to 4 with  $P_{\max} = 10$  dBm.

of the elements at the RIS becomes larger (from 20 to 40), the gap between the rate of the SU achieved by the proposed GLD method and that of the SDP method becomes more obvious. The reason for the large gap between these two methods is that the interference part in P2 becomes non-negligible when  $N$  becomes larger. The proposed GLD method can optimize the numerator and denominator in P2 jointly, achieved by the adjustment of beamforming vector of the S-AP and the reflecting coefficients at the RIS. However, the performance of SDP method decreases sharply for only optimizing the numerator in P2. Therefore, our proposed GLD algorithm can have the obvious gain over the compared SDP on the achievable rate of the SU.

Fig. 8 shows the SE performance of the proposed GLD method and the compared SDP method with the number of primary networks ranges from 2 to 4 as the number of the elements of RIS increases from 1 to 40. As the number of primary networks increases in Fig. 8, the SE performance of system decreases sharply for more interference introduced in the denominator of P1 and more constraints added in (13b). Besides, increasing the number of the elements of RIS can improve SE with different number of the primary networks in both methods. However, the proposed GLD method can obtain better gain from the increasing of  $N$  than the compared SDP method.

As Fig. 9 is shown, compared with the SSS without RIS (w/o RIS), RIS can provide significant gain on the EE performance in the SSS with multiple primary networks, which can be illustrated with Gap 1, Gap 2 and Gap 3. As we increase the maximum transmit power from 6 dBm to

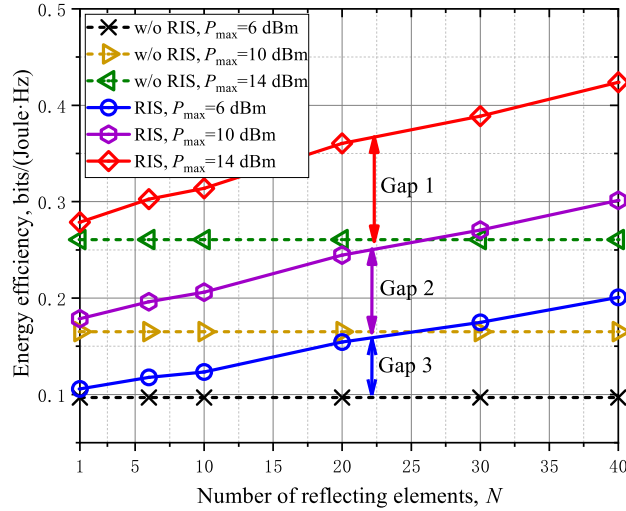


Fig. 9. The energy efficiency of the secondary network obtained by the GLD method with  $J = 2$ .

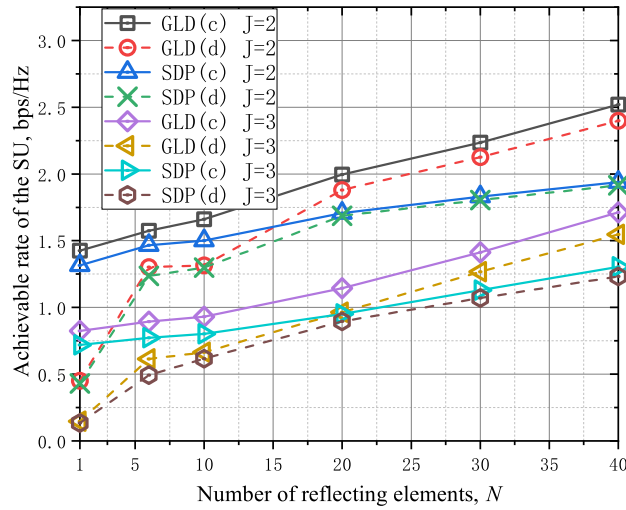


Fig. 10. The achievable rates of the SU obtained by the GLD method and the compared SDP method for the phase discretization of  $\hat{\theta}$  on the NPSP with  $P_{\max} = 10$  dBm and 2 bits used to quantify the phase shifts where (c) and (d) mean continuous value and discrete value for  $\hat{\theta}$ , respectively.

14 dBm, the enhancement about the EE performance of the secondary network by RIS becomes larger (from Gap 3 to Gap 1). Besides, the increasing on the number of reflecting elements can strengthen the advantage of RIS on improving EE performance, which implies that the SE enhancement from increasing  $N$  is dominant than the cost of the additional power on the RIS.

For the practical consideration about the reflecting coefficients, the proposed NPSP is utilized to quantize the phase shifts of the reflecting coefficients  $\hat{\theta}$  at the RIS for the proposed GLD method and the compared SDP method. Fig. 10 shows the performance of GLD and SDP with

the embedded NPSP for the phase discretization of  $\hat{\theta}$ . The discretization of  $\hat{\theta}$  decreases the achievable rate of the SU slightly for the proposed GLD method and the compared SDP method with the number of primary network  $J = 2$  or 3. Besides, the achievable rate of SU about the proposed GLD method with NPSP embedded for the phase discretization of  $\hat{\theta}$  is still better than that of compared SDP method in the same case. It is worth noting that the achievable rate of the SU with the phase discretization of  $\hat{\theta}$  encounters the sharp decreasing with a small  $N$ , compared with that of continuous value of  $\hat{\theta}$ . When  $N$  is small, the phase discretization of  $\hat{\theta}$  may result in the invalidation about the constraints in (27c).

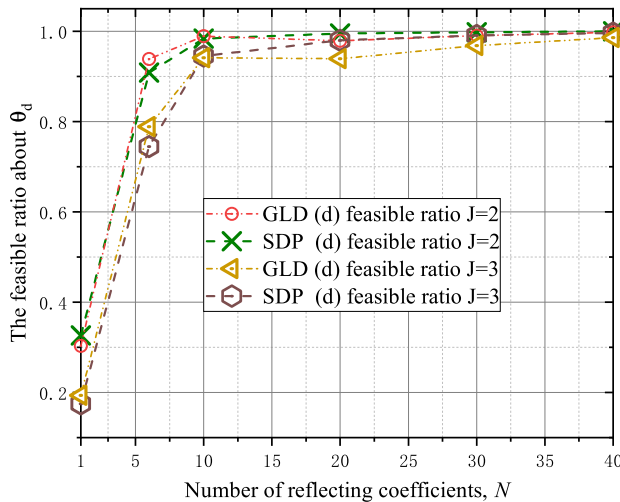


Fig. 11. The feasible ratio about the phase discretization of  $\hat{\theta}$  with the NPSP as the number of reflecting elements  $N$  increases with  $P_{\max} = 10$  dBm and (d) denoting discrete value for  $\hat{\theta}$ .

The probabilities about obtaining the feasible solution for the phase discretization of  $\hat{\theta}$  are shown in Fig. 11, which can explain the degradation about the performance of the phase discretization of  $\hat{\theta}$  with a small  $N$ . When  $N$  is larger than 10, the feasible ratio is over 90 percents, which can ensure that the phase discretization of  $\hat{\theta}$  has little loss on the performance of the system. Besides, the feasible ratio approaches to 1 as the number of reflecting coefficients  $N$  becomes larger.

## VI. CONCLUSION

In this paper, the problem about improving the SE and EE performance of the secondary network in the SSS assisted by the RIS with multiple primary networks was investigated. As the simulation results showed, the SE performance of the GLD method can well approach that of the optimal DES with a small gap. Although more primary networks would decrease the SE

performance of the SU due to more interference introduced in the system, our proposed GLD method can improve the achievable rate of the SU compared with the traditional SDP method. Besides, RIS can elevate the EE performance of the secondary network by passive beamforming, where the extra power consumption to support the RIS in working mode is limited. Moreover, the NPSP algorithm was proposed to realize the discretization of phase shifts about the reflecting coefficients at the RIS in practical system. By quantizing the phase shifts of the reflecting coefficients at the RIS to the nearest discrete point, NPSP experienced little loss on the SE performance in the SSS with multiple primary networks. The RIS can amplify the effective signals and reduce the interference of the SU by empowering the radio environments of wireless channels, which improves the SE and EE performance of the secondary network in the SSS with multiple primary networks significantly.

## REFERENCES

- [1] Z. Zhang, Y. Xiao, Z. Ma, M. Xiao, Z. Ding, X. Lei, G. K. Karagiannidis, and P. Fan, "6G wireless networks: Vision, requirements, architecture, and key technologies," *IEEE Veh. Technol. Mag.*, vol. 14, no. 3, pp. 28–41, 2019.
- [2] S. Aggarwal, N. Kumar, and S. Tanwar, "Blockchain-envisioned UAV communication using 6G networks: Open issues, use cases, and future directions," *IEEE Internet Things J.*, vol. 8, no. 7, pp. 5416–5441, 2021.
- [3] A. Goldsmith, S. A. Jafar, I. Maric, and S. Srinivasa, "Breaking spectrum gridlock with cognitive radios: An information theoretic perspective," *Proc. IEEE*, vol. 97, no. 5, pp. 894–914, 2009.
- [4] M. M. Sohel, M. Yao, T. Yang, and J. H. Reed, "Spectrum access system for the citizen broadband radio service," *IEEE Commun. Mag.*, vol. 53, no. 7, pp. 18–25, 2015.
- [5] W. Tang, M. Z. Chen, X. Chen, J. Y. Dai, Y. Han, M. Di Renzo, Y. Zeng, S. Jin, Q. Cheng, and T. J. Cui, "Wireless communications with reconfigurable intelligent surface: Path loss modeling and experimental measurement," *IEEE Trans. Wireless Commun.*, vol. 20, no. 1, pp. 421–439, 2021.
- [6] Q. Wu and R. Zhang, "Towards smart and reconfigurable environment: Intelligent reflecting surface aided wireless network," *IEEE Commun. Mag.*, vol. 58, no. 1, pp. 106–112, January 2020.
- [7] Y. Liu, Y. Zhang, X. Zhao, S. Geng, P. Qin, and Z. Zhou, "Dynamic-controlled ris assisted multi-user MISO downlink system: Joint beamforming design," *IEEE Trans. Green Commun. Netw.*, pp. 1–1, 2021.
- [8] L. Du, W. Zhang, J. Ma, and Y. Tang, "Reconfigurable intelligent surfaces for energy efficiency in multicast transmissions," *IEEE Trans. Veh. Technol.*, vol. 70, no. 6, pp. 6266–6271, 2021.
- [9] K. D. Gupta, R. Nigam, D. K. Sharma, and S. K. Dhurandher, "LSTM based energy-efficient wireless communication with reconfigurable intelligent surfaces," *IEEE Trans. Green Commun. Netw.*, pp. 1–1, 2021.
- [10] L. Dai, B. Wang, M. Wang, X. Yang, J. Tan, S. Bi, S. Xu, F. Yang, Z. Chen, M. D. Renzo, C.-B. Chae, and L. Hanzo, "Reconfigurable intelligent surface-based wireless communications: Antenna design, prototyping, and experimental results," *IEEE Access*, vol. 8, pp. 45 913–45 923, 2020.
- [11] C. Pan, H. Ren, K. Wang, W. Xu, M. Elkashlan, A. Nallanathan, and L. Hanzo, "Multicell MIMO communications relying on intelligent reflecting surfaces," *IEEE Trans. Wireless Commun.*, vol. 19, no. 8, pp. 5218–5233, 2020.

- [12] Z. Zhang and L. Dai, "A joint precoding framework for wideband reconfigurable intelligent surface-aided cell-free network," *IEEE Trans. Signal Process.*, vol. 69, pp. 4085–4101, 2021.
- [13] G. Zhou, C. Pan, H. Ren, K. Wang, and A. Nallanathan, "Intelligent reflecting surface aided multigroup multicast MISO communication systems," *IEEE Trans. Signal Process.*, vol. 68, pp. 3236–3251, 2020.
- [14] L. Mohjazi, S. Muhaidat, Q. H. Abbasi, M. A. Imran, O. A. Dobre, and M. Di Renzo, "Battery recharging time models for reconfigurable intelligent surfaces-assisted wireless power transfer systems," *IEEE Trans. Green Commun. Netw.*, pp. 1–1, 2021.
- [15] W. Yan, X. Yuan, Z.-Q. He, and X. Kuai, "Passive beamforming and information transfer design for reconfigurable intelligent surfaces aided multiuser MIMO systems," *IEEE J. Sel. Areas Commun.*, vol. 38, no. 8, pp. 1793–1808, 2020.
- [16] H. Liu, X. Yuan, and Y.-J. A. Zhang, "Reconfigurable intelligent surface enabled federated learning: A unified communication-learning design approach," *IEEE Trans. Wireless Commun.*, vol. 20, no. 11, pp. 7595–7609, 2021.
- [17] T. Zhang and S. Mao, "Energy-efficient federated learning with intelligent reflecting surface," *IEEE Trans. Green Commun. Netw.*, pp. 1–1, 2021.
- [18] B. Yang, X. Cao, C. Huang, C. Yuen, L. Qian, and M. D. Renzo, "Intelligent spectrum learning for wireless networks with reconfigurable intelligent surfaces," *IEEE Trans. Veh. Technol.*, vol. 70, no. 4, pp. 3920–3925, 2021.
- [19] C. Huang, R. Mo, and C. Yuen, "Reconfigurable intelligent surface assisted multiuser miso systems exploiting deep reinforcement learning," *IEEE J. Sel. Areas Commun.*, vol. 38, no. 8, pp. 1839–1850, 2020.
- [20] X. Tan, Z. Sun, J. M. Jornet, and D. Pados, "Increasing indoor spectrum sharing capacity using smart reflect-array," in *2016 IEEE International Conference on Communications (ICC)*, 2016, pp. 1–6.
- [21] X. Guan, Q. Wu, and R. Zhang, "Joint power control and passive beamforming in IRS-assisted spectrum sharing," *IEEE Commun. Lett.*, vol. 24, no. 7, pp. 1553–1557, 2020.
- [22] L. Zhang, Y. Wang, W. Tao, Z. Jia, T. Song, and C. Pan, "Intelligent reflecting surface aided MIMO cognitive radio systems," *IEEE Trans. Veh. Technol.*, vol. 69, no. 10, pp. 11 445–11 457, 2020.
- [23] L. You, J. Xiong, Y. Huang, D. W. K. Ng, C. Pan, W. Wang, and X. Gao, "Reconfigurable intelligent surfaces-assisted multiuser MIMO uplink transmission with partial csi," *IEEE Trans. Wireless Commun.*, vol. 20, no. 9, pp. 5613–5627, 2021.
- [24] D. Xu, X. Yu, Y. Sun, D. W. K. Ng, and R. Schober, "Resource allocation for IRS-assisted full-duplex cognitive radio systems," *IEEE Trans. Commun.*, vol. 68, no. 12, pp. 7376–7394, 2020.
- [25] Q. Wu and R. Zhang, "Beamforming optimization for wireless network aided by intelligent reflecting surface with discrete phase shifts," *IEEE Trans. Commun.*, vol. 68, no. 3, pp. 1838–1851, 2020.
- [26] H. Liu, X. Yuan, and Y. J. Zhang, "Statistical beamforming for FDD downlink massive MIMO via spatial information extraction and beam selection," *IEEE Trans. Wireless Commun.*, vol. 19, no. 7, pp. 4617–4631, 2020.
- [27] J. Yuan, Y.-C. Liang, J. Joung, G. Feng, and E. G. Larsson, "Intelligent reflecting surface-assisted cognitive radio system," *IEEE Trans. Commun.*, vol. 69, no. 1, pp. 675–687, 2021.
- [28] H. Guo, Y.-C. Liang, J. Chen, and E. G. Larsson, "Weighted sum-rate maximization for reconfigurable intelligent surface aided wireless networks," *IEEE Trans. Wireless Commun.*, vol. 19, no. 5, pp. 3064–3076, 2020.
- [29] Z. Yang, M. Chen, W. Saad, W. Xu, M. Shikh-Bahaei, H. V. Poor, and S. Cui, "Energy-efficient wireless communications with distributed reconfigurable intelligent surfaces," *IEEE Trans. Wireless Commun.*, pp. 1–1, 2021.